Shape coexistence and lifetime measurement in ^{187}Tl nucleus

S. K. Chamoli,[1] P. Joshi,[1,2] A. Kumar,[1] Rajesh Kumar,[1] R. P. Singh,[2] S. Muralithar,[2] R. K. Bhowmik,[2] and I. M. Govil[1]
[1]*Department of Physics, Panjab University, Chandigarh 160014, India*
[2]*Nuclear Science Centre, Post Box No. 10502, New Delhi 110067, India*
(Received 25 March 2004; published 31 May 2005)

The lifetime measurements are done for different quasiparticle bands in neutron-deficient ^{187}Tl nucleus through the recoil distance Doppler shift technique. A sudden change in the transition quadrupole moment is observed for both positive and negative parity prolate bands as one moves from lower spins to higher spins, indicating a major shape transitions in this nucleus. The prolate-oblate shape coexistence picture of this nucleus is discussed in the light of the extracted transition quadrupole moments. For the negative parity $\pi h_{9/2}$ band the transition quadrupole moment for the low K (3/2) prolate sequence is found to be higher than that of the high K (9/2) oblate sequence. The total Routhian surface calculations are done within the framework of the cranked Hartree-Fock-Bogoliubov model to analyze the shape coexistence picture theoretically. The theoretical predictions are found to be in close agreement with the experimental observations. The existence of a superdeformed band is also predicted for the nucleus.

DOI: 10.1103/PhysRevC.71.054324 PACS number(s): 21.10.Tg, 21.10.Ky, 27.70.+q

I. INTRODUCTION

The neutron-deficient nuclei around $Z = 82$ shell closure exhibit rich structural properties of topical interest. In these nuclei for a well-deformed prolate shape the proton Fermi level is below the low-K orbitals of $h_{9/2}$ ($K = 1/2$, 3/2) and $i_{13/2}$ ($K = 1/2$) bands, whereas the Fermi level is above the high $K = 9/2$ and 13/2 orbitals of the $h_{9/2}$ and $i_{13/2}$ bands respectively. Therefore, the low-K intruder states well above the Fermi level have a strong tendency to drive the nucleus toward higher prolate deformations, whereas the high-K states below the Fermi level drive the nucleus toward more spherical or moderate oblate deformations. The nuclei in this mass region are therefore expected to exhibit the shape coexistence phenomena in their structure, which in fact is observed at low spins in even-even $^{180-190}$Hg isotopes [1–10] and also in even-even ^{186,188}Pb isotopes [11,12]. The best way to understand the type of orbitals responsible for giving this coexistence picture in the even-even nuclei is to investigate the neighboring odd mass nuclei, with the odd nucleon used as a probe. The high spin structure of a number of intervening neutron-deficient thallium nuclei having their Z values just one less than the closed shell structure ($Z = 82$) have been probed experimentally [13–18] with this motivation. The oblate bands based on $\pi h_{9/2}[505]9/2^-$ and the $\pi i_{13/2}[606]13/2^+$ orbitals coupled to the oblate ground state of Hg have been observed to form the negative parity and the positive parity ground-state bands respectively in all the light Tl nuclei studied so far [15–17]. At high spins the low-K, $\pi i_{13/2}[660]1/2^+$, and $\pi h_{9/2}[532]3/2^-$ orbitals coupled to the prolate Hg core are seen in ^{185,187}Tl, whereas for the heavier Tl nuclei, only one prolate band associated with $\pi i_{13/2}[660]1/2^+$ is found to compete with the oblate ground state band. Porquet *et al.* [14] predict this nonobservation of a prolate $\pi h_{9/2}$ structure in other heavier Tl nuclei ($A \geqslant 189$) as resulting from the pushing up of this structure in energy as a result of the significant loss in pairing correlation of the core caused by the Pauli blocking of the $\pi h_{9/2}$ structure in the presence of the prolate Hg core of $(\pi h_{9/2})^2$ configuration. Conversely, Lane *et al.* [17] relate this absence of prolate $\pi h_{9/2}$ structure at high spins in heavier Tl nuclei, with the decrease in the deformation of this band in moving away from the neutron midshell ($N = 104$). As at high spins the centrifugal and the Coriolis potential added to the ground-state potential produce relatively lower energy for the states with large deformations, so this low deformed $\pi h_{9/2}$ prolate structure will be less favorable at high spins. In the cases of ^{185}Tl ($N = 104$) and ^{187}Tl ($N = 106$) the prolate $h_{9/2}$ configuration is based on the $K = 3/2$ orbital, whereas for the other heavier isotopes it is based on the $K = 1/2$ orbital. Lane *et al.* [17] have predicted this to be because of the higher deformation of $K = 3/2$ configuration as compared to the $K = 1/2$ near the neutron midshell and hence more favorable at higher spins. Thus to confirm the prolate-oblate shape coexistence and the predictions of the higher deformations for the $K = 3/2, \pi h_{9/2}$ configuration as compared to the $K = 1/2, \pi h_{9/2}$, it is important to do the shape studies in the ^{187}Tl nucleus. As the quadrupole moment is a direct signature of the intrinsic deformation and hence the shape of the nucleus, the lifetime measurements are done for different quasiproton bands observed in ^{187}Tl using the recoil distance Doppler shift method (RDM). The experimental results are compared with the self-consistent total Routhian surface (TRS) calculations within the framework of cranked Hartree-Fock-Bogoliubov (CHFB) model.

II. EXPERIMENTAL DETAILS

The high-spin states of ^{187}Tl were populated using the heavy-ion fusion evaporation reaction ^{159}Tb(^{32}S, $4n$)^{187}Tl at a beam energy of 154 MeV. A good-quality ^{32}S beam was delivered by the 15 UD Pelletron at Nuclear Science Center (NSC), New Delhi. The in-beam excitation function was done and 154 MeV beam energy was found to yield the maximum cross section for the reaction used. Using the energy separation of the unshifted and the corresponding shifted γ-ray peaks,

TABLE I. Experimental results for different γ transitions in proton quasiparticle $\pi h_{9/2}$ band in ^{187}Tl.

S. No.	Energy (keV)	Spin (I_i^π)	Lifetime (ps)	B(E2) (e^2b^2)	Q_t (eb)	β_2	Side-feeding lifetime (ps)
1.	662.3	$\frac{13}{2}^-$	$2.9 \pm {}^{0.3}_{0.3}$	$0.22 \pm {}^{0.08}_{0.05}$	$2.6 \pm {}^{0.3}_{0.3}$	$0.10 \pm {}^{0.02}_{0.02}$	<0.4
2.	451.1	$\frac{17}{2}^-$	$28.3 \pm {}^{2.9}_{3.2}$	$0.15 \pm {}^{0.02}_{0.02}$	$2.1 \pm {}^{0.1}_{0.1}$	$0.07 \pm {}^{0.01}_{0.01}$	<0.1
3.	427.3	$\frac{21}{2}^-$	$3.3 \pm {}^{1.0}_{0.8}$	$1.63 \pm {}^{0.30}_{0.25}$	$6.4 \pm {}^{0.7}_{0.6}$	$0.22 \pm {}^{0.02}_{0.02}$	<4.6
4.	488.3	$\frac{25}{2}^-$	<1.6	>1.70	>6.6	>0.23	—

it is found that the beam has imparted a recoil velocity of $v/c \sim 1.3\%$ to the residual nuclei in the forward direction. A self-supporting target foil of ^{159}Tb of thickness 1.1 mg/cm^2 and a stopper foil of gold of thickness 10 mg/cm^2 were mounted and stretched on two identical metal cones in the NSC plunger device. To detect the emitted γ rays the GDA setup at NSC, consisting of 12 Compton-suppressed HPGe detectors and a 14-element BGO multiplicity filter, was used in conjunction with the RDM device. The detectors in he GDA setup are arranged in three different rings to make an angle of 50°, 99°, and 144° with the direction of the beam. The data was collected for 22 target-stopper distances ($D_{T\text{-}S}$) ranging from 12 to 10,000 μm. The data at a distance of 10,000 μm is taken to include the effect of any unknown transition of long lifetime feeding the levels of the band. The distance between the target and the stopper foils is measured by the capacitance method, described earlier [19]. The minimum distance between the target and the stopper is found to be 12 μm. The data were collected in the singles mode with the condition that at least two BGO multiplicity detectors ($M \geqslant 2$) should fire in coincidence with one of the HPGe detectors. The BGO multiplicity gating helps to reduce the background contribution coming from Coulomb excitation and the radioactivity and so on.

III. DATA ANALYSIS

The data obtained with all the four detectors at each angle, are gain matched and added to form the raw spectrum. The fitting of the spectra is done to find the area of the unshifted (U) and the corresponding shifted (S) peaks for all the target-stopper distances. The area of the unshifted peak is normalized to the total intensity (sum of the unshifted and the corrected shifted intensity) and also to the intensity of the Coulomb excited gold peak at 547 keV. The local fluctuations in the error bars for different γ transitions are because of the fluctuations in the fitting error of the γ-ray peaks mainly because the statistical error in the present data was found to be small relative to the fitting error. The resulting intensity decay curves of the unshifted γ transitions have been analyzed with the computer program LIFETIME [20] to extract the level lifetimes. The program determines the level population by direct solution of the Bateman equations and calculates the values of the shifted and the unshifted intensities for each γ transition. For this purpose, at each level two types of feeding is considered in the program, namely the cascade feeding from the above and the side feeding, except for the highest level for which the feeding from the top is assumed through an unknown rotational band of constant quadrupole moment. The quadrupole moment of this modeled rotational band and the initial population of the highest level are treated as variable parameters in the program. For each γ transition in the decay cascade the initial level population and the transition probability are given as inputs in the program. Moreover, for each side feeding γ transition the initial level population and the transition rates are given as input. Initially the side feeding lifetimes were assumed to be smaller than the lifetimes of the levels being fed by them. During the least-squars fitting of the data, the intensity of side feeding is assumed by the program in such a way so as to conserve the total intensity at each distance, whereas the initial population and transition rates for each modeled feeding level are treated as free parameters. Finally, the program assumes such values of side feeding level lifetimes that give the best fit of the data. Such assumed side feeding level lifetimes for different levels in the negative parity $\pi h_{9/2}$ and the positive parity $\pi i_{13/2}$ bands are tabulated in the last column of Tables I and II respectively. The LIFETIME

TABLE II. Experimental results for different γ transitions in proton quasiparticle $\pi i_{13/2}$ band in ^{187}Tl.

S. No.	Energy (keV)	Spin (I_i^π)	Lifetime (ps)	$B(E2)$ (e^2b^2)	Q_t (eb)	β_2	Side-feeding lifetime (ps)
1.	392.8	$\frac{17}{2}^+$	$64.2 \pm {}^{7.7}_{8.5}$	$0.11 \pm {}^{0.01}_{0.02}$	$1.8 \pm {}^{0.1}_{0.1}$	$0.07 \pm {}^{0.01}_{0.01}$	<0.1
2.	285.5	$\frac{21}{2}^+$	$35.6 \pm {}^{3.4}_{3.4}$	$1.06 \pm {}^{0.10}_{0.10}$	$5.6 \pm {}^{0.3}_{0.3}$	$0.19 \pm {}^{0.02}_{0.02}$	<2.5
3.	366.3	$\frac{25}{2}^+$	$5.2 \pm {}^{1.0}_{0.8}$	$2.04 \pm {}^{0.50}_{0.32}$	$7.7 \pm {}^{0.9}_{0.6}$	$0.27 \pm {}^{0.02}_{0.02}$	<4.1
4.	442.6	$\frac{29}{2}^+$	<2.0	>2.29	>8.1	>0.28	—

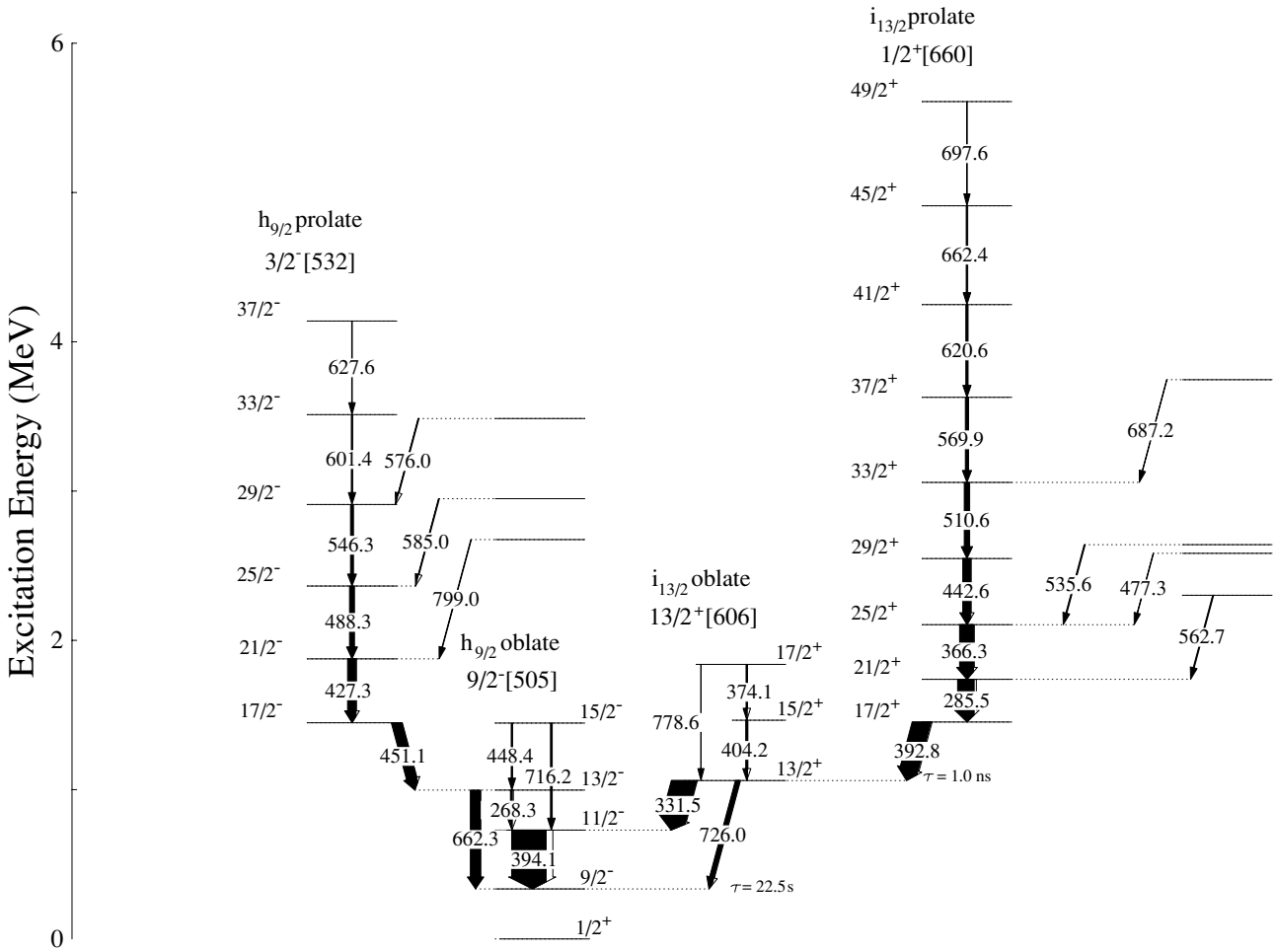

FIG. 1. Partial level scheme of ^{187}Tl relevant to this work showing different quasiproton bands for which lifetime measurement is done. The widths of the transitions are proportional to the γ-ray intensities. The full level scheme appears in Ref. [17].

program also includes corrections to the raw data for the finite target thickness, position- and velocity-dependent solid angle, and for the attenuation of γ-ray angular distribution resulting from the nuclear deorientation effect [21]. In presence of the nuclear deorientation, the total intensity of a stretched $E2$ transition decreases with increasing target to stopper distance. But as none of the γ transitions considered in the present data showed significant deviations with increasing target-stopper distance from the mean value of total intensity, so the nuclear deorientation effect was found to be small. This effect is further reduced because of the high spins of the states. Hence in the present data the correction for the nuclear deorientation effect was not required. Also, because of the small target thickness ($\sim$1 mg/cm^2), the spread in the velocity ($\Delta\beta$) of the recoils coming out of it was found to be small ($\sim$0.003%). The uncertainties in the measured lifetimes have been found by using a subroutine, MINUIT [22], included in the program. It finds the true parameter errors by examining the behavior of the χ^2 function over the unit interval on both side of the minimum.

IV. RESULTS AND DISCUSSION

The extensive level scheme for this nucleus exists from the previous spectroscopic studies [15–17]. The partial level scheme relevant to this work is shown in Fig. 1. The low energy spectra at a forward angle of 50° with respect to the beam direction, containing the shifted (S) and the unshifted (U) peaks of γ-ray transitions of interest at four target to stopper distances are illustrated in Fig. 2. The results of the lifetime measurement for the $h_{9/2}$ and $i_{13/2}$ bands are summarized in Tables I and II respectively. From the measured lifetimes, the BE(2) values and the reduced transition quadrupole moment (Q_t) are calculated using the rotational model with the following relations:

$$B(E2) = \frac{0.82}{\tau E_\gamma^5 (1+\alpha_\tau)} |e^2 b^2| \qquad (1)$$

and

$$Q_t^2 = \left(\frac{16\pi}{5}\right) \frac{B(E2; I \rightarrow I-2)}{\langle I2K0|I-2K\rangle^2}, \qquad (2)$$

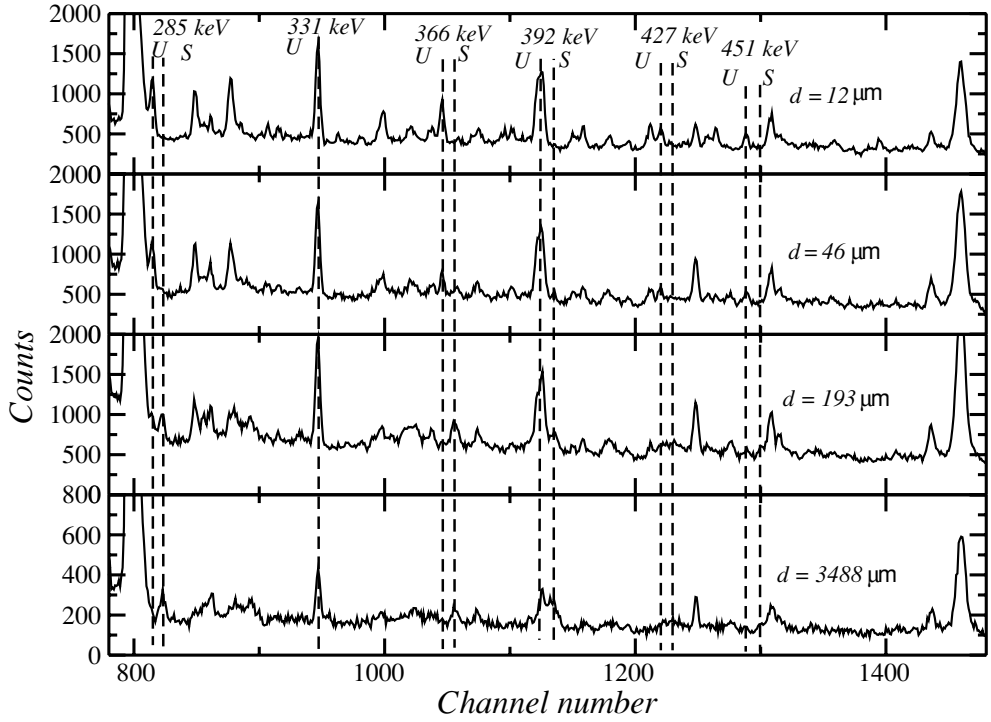

FIG. 2. A portion of the raw spectrum showing the shifted (S) and unshifted (U) peaks of few γ transitions of interest in ^{187}Tl at four different target-stopper distances ($D_{T\text{-}S}$) at an angle of 50° with respect to the beam direction.

where τ is the lifetime (in picoseconds), E_γ is the γ-ray transition energy (in mega-electron-volts), and α is the conversion coefficient. For the $h_{9/2}$ bands, $K = 3/2$ and 9/2 are used for the prolate and the oblate rotational sequences respectively, whereas for the $i_{13/2}$ prolate band $K = 1/2$ is used. The intensity decay curves for the unshifted γ-ray transitions observed for the $\pi h_{9/2}$ and $\pi i_{13/2}$ bands are shown in Figs. 3 and 4 respectively. For the $h_{9/2}$ prolate band no decay curve could be obtained for 546.3-keV ($29/2^- \rightarrow 25/2^-$) transition, as it is heavily mixed with the 547-keV Coulomb excited gold peak. Similarly, the 510.6-keV ($33/2^+ \rightarrow 29/2^+$) transition in the $i_{13/2}$ prolate band is heavily mixed with the 511.0-keV annihilation peak and hence no decay curve could be obtained for this transition also. The 392.8-keV transition ($\tau \sim 64$ ps), connecting the positive parity prolate band to the positive parity oblate band, is heavily mixed with the 394.1-keV microseconds lifetime transition of the $h_{9/2}$ oblate band [17]. But because of the huge difference in their lifetimes it was possible to resolve their shifted components; hence the area of the shifted component of 392.8-keV transition is used for the lifetime analysis. For the most intense isomeric γ-ray transitions of 331.5 keV of the oblate $i_{13/2}$ band and 394.1 keV of the oblate $h_{9/2}$ band (Fig. 1), with lifetimes of the order of nanoseconds and microseconds respectively, no shift could be obtained in the present experiment.

For the observed transitions in the $h_{9/2}$ and the $i_{13/2}$ bands the extracted Q_t values are plotted as a function of the spin in Fig. 5. It is observed from Fig. 5 that the value of transition quadrupole moment for the $h_{9/2}$ band decreases slightly from 2.6 to 2.1 eb as one moves from the spin $13/2^-$ to $17/2^-$ and then changes suddenly to 6.4 eb at spin $21/2^-$. This increase of almost three times in the value of the quadrupole moment is an indication of a major shape change taking place in the structure of ^{187}Tl in this configuration between these two spins. According to the Nilsson diagram the low K (3/2) configuration of $h_{9/2}$ band is highly down sloping as a function of deformation and acts as an intruder state coming from above the $Z = 82$ shell closure, whereas the high K (9/2) configuration slopes upward and hence has the tendency to drive the nucleus toward spherical or small oblate shapes. The observed small drop of the quadrupole moment of the 451.1-keV linking transition ($17/2^- \rightarrow 13/2^-$) of the $h_{9/2}$ band at the oblate-prolate changeover is probably because of the mixing of the prolate band with the ground-state oblate band as the odd particle changes its orbit from oblate to prolate. The observed sharp gain in the Q_t value between $17/2^-$ and $21/2^-$ spins indicates the stretching of the nucleus as soon as it acquires a prolate structure.

For the positive parity prolate $i_{13/2}$ band, it is observed from Fig. 5 that at low spins ($I \leqslant 21/2^+$), the transition quadrupole moment is less than that for the negative parity $h_{9/2}$ band. But, at high spins ($I \geqslant 21/2^+$) no such comparison is possible because of insufficient data. Q_t for this positive parity ($i_{13/2}$) band increases from a small value of 1.8 eb at $17/2^+$ to 5.6 eb at $21/2^+$, which shows a threefold change in its value between these two spins. After this it further increases to a value of 7.7 eb at $25/2^+$. It therefore confirms that the nucleus acquires major centrifugal stretching right in the beginning of the shape change from oblate to prolate and then tends to attain an equilibrium deformation. This process occurs if the

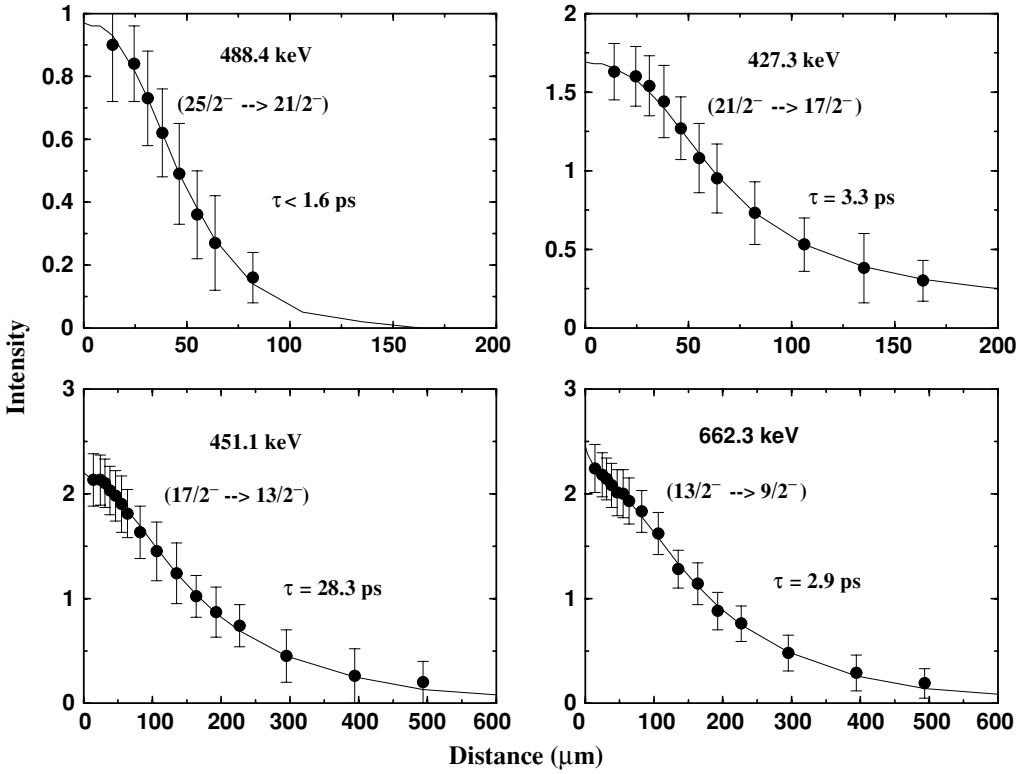

FIG. 3. The intensity decay curves for the unshifted γ-ray transitions of prolate and oblate decay sequences in $\pi h_{9/2}$ band in ^{187}Tl.

potential energy as a function of deformation has a minimum at small deformation and a shoulder or a second minimum at a larger deformation and at somewhat larger energy. The lower yrast states are then confined in the first well at a small deformation, but at higher spins the centrifugal potential added to the ground-state potential produces a relatively lower energy in the second well.

The high-spin features of the prolate bands can be more clearly explained through the plot of the aligned angular momentum in the rotating frame of reference. For this purpose the alignment curves as a function of the rotational frequency are plotted in Fig. 6 for the prolate $h_{9/2}$ and $i_{13/2}$ bands in ^{187}Tl. The alignment curve for the prolate ground-state band in ^{186}Hg is also shown for comparison. It is clear from the figure that the alignment curve for both the prolate bands in ^{187}Tl have an almost identical behavior with initial gain at low rotational frequencies and then a nearly constant alignment at intermediate frequencies before the band crossing at 0.28 MeV for the $h_{9/2}$ band. The gain of alignment for the two bands at low frequencies is attributed to the change from slightly oblate ground state to a more deformed prolate shape, which is also indicated by the measured lifetimes and quadrupole moments. In the band crossing region the nature of the alignment curve for the $i_{13/2}$ prolate band in ^{187}Tl is different from the $h_{9/2}$ band. The band crossing corresponding to the alignment of a pair of $i_{13/2}$ neutrons in this mass region, occurs at $\hbar\omega \sim 0.28$ MeV in the $h_{9/2}$ band of ^{187}Tl and also in the ground state band of ^{186}Hg [17], while it is found to be absent or rather delayed to higher frequencies for the $i_{13/2}$ band of ^{187}Tl, which looks very collective over the entire range of observed frequencies. From the previous studies in ^{177}Re [23], ^{171,173}Ta [24,25] , ^{179}Ir [26], and ^{183}Au [27], the delay in the crossing frequency observed for some bands corresponding to their nearest even-even neighbors is the result of their higher deformation. Therefore, the same crossing frequency ($\hbar\omega \sim 0.28$ MeV) for the $h_{9/2}$ band in ^{187}Tl and the ground-state band in ^{186}Hg [28] indicates a similar deformation for them but a comparatively higher deformation for the $i_{13/2}$ band in ^{187}Tl. The nearly equal $B(E2)$ values within the experimental uncertainty for the ground-state band in ^{186}Hg [28] and for the negative parity, positive signature $\pi h_{9/2}$ band in ^{187}Tl indicate a similar deformation in the two cases. The observed higher value of the average transition quadrupole moment for the $i_{13/2}$ band (7.2 eb) than the $h_{9/2}$ band (6.5 eb) clearly justifies the delay of crossing frequency in $i_{13/2}$ prolate band as compared to the $h_{9/2}$ band.

To understand the phenomena of shape coexistence theoretically, the TRS calculations have been done within the cranked Hartree-Fock-Bogoliubov (CHFB) framework [29,30] for the positive parity and the negative parity ground-state configurations in ^{187}Tl. For these calculations the average mean field is taken to be a rotating Wood–Saxon potential [31,32] with monopole type of pairing interaction. The pairing $\triangle (= \triangle_n = \triangle_p)$ and the Fermi level λ are found self-consistently using the Bardeen-Cooper-Schrieffer (BCS) equations [33]. To include the microscopic quantal effects in the single-particle energy the Strutinsky shell corrections [34] are applied. This corrected total energy of the nucleus

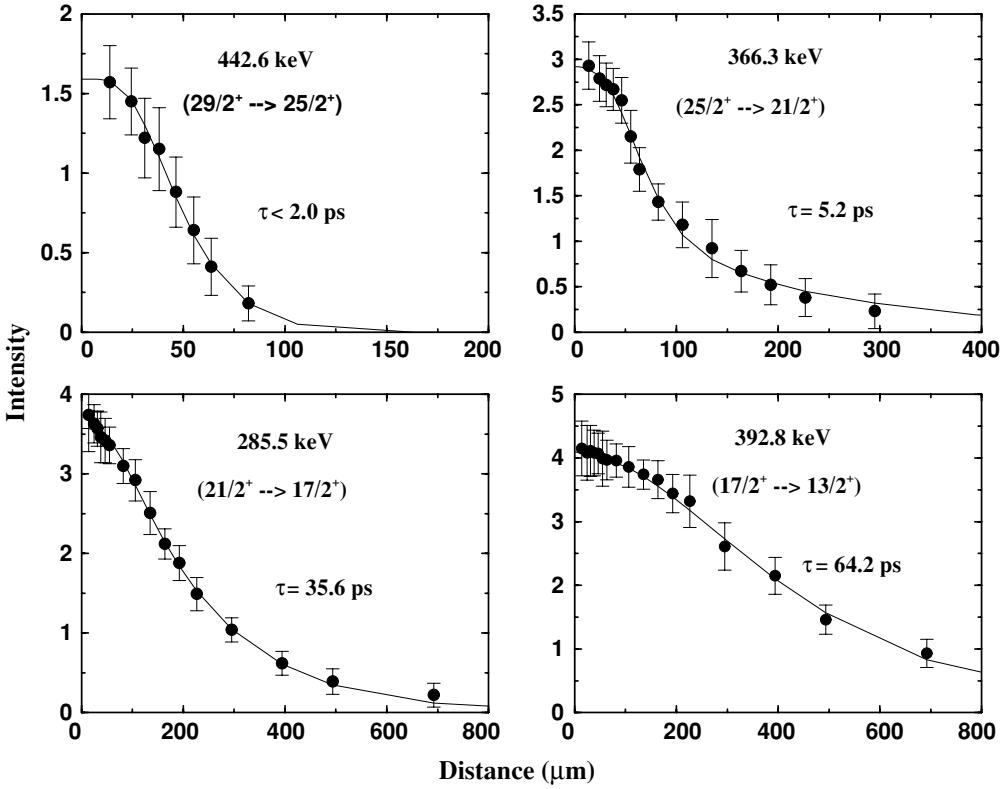

FIG. 4. The intensity decay curves for the unshifted γ-ray transitions of $\pi i_{13/2}[660]1/2^+$ band in ^{187}Tl.

in the rotating frame is then minimized with respect to the three deformation parameters β_2, γ, and β_4. The calculated β_2 and γ deformations at different rotational frequencies for the negative parity, positive signature $\pi h_{9/2}$ and positive parity, positive signature $\pi i_{13/2}$ ground-state bands are shown in Figs. 7(a) and 7(b) respectively. From the figures it is clear that for the negative parity $h_{9/2}$ band at zero rotational frequency, the nucleus assumes an oblate shape with minimum in the potential energy surfaces at $\beta_2 \sim 0.15$, $\gamma \sim -60^\circ$. For the positive parity $i_{13/2}$ band also at zero rotational frequency the nucleus assumes an oblate shape with $\beta_2 \sim 0.08$, $\gamma \sim -60^\circ$. This is consistent with our experimental observations for both the bands. However, interesting structural changes are observed with an increase in rotational frequency

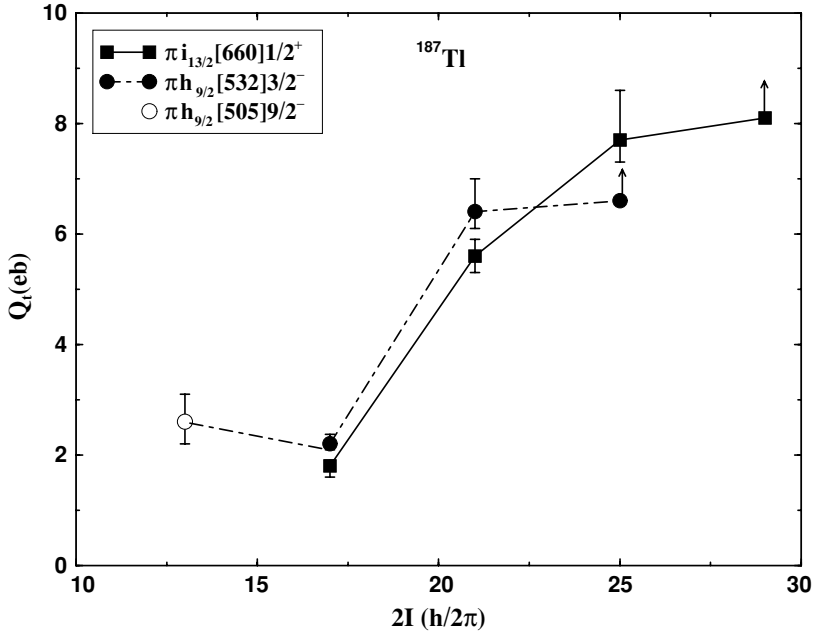

FIG. 5. Plot of the variation of observed transition quadrupole moment (Q_t) with spin (I) for both the $\pi h_{9/2}$ and $\pi i_{13/2}$ bands in ^{187}Tl.

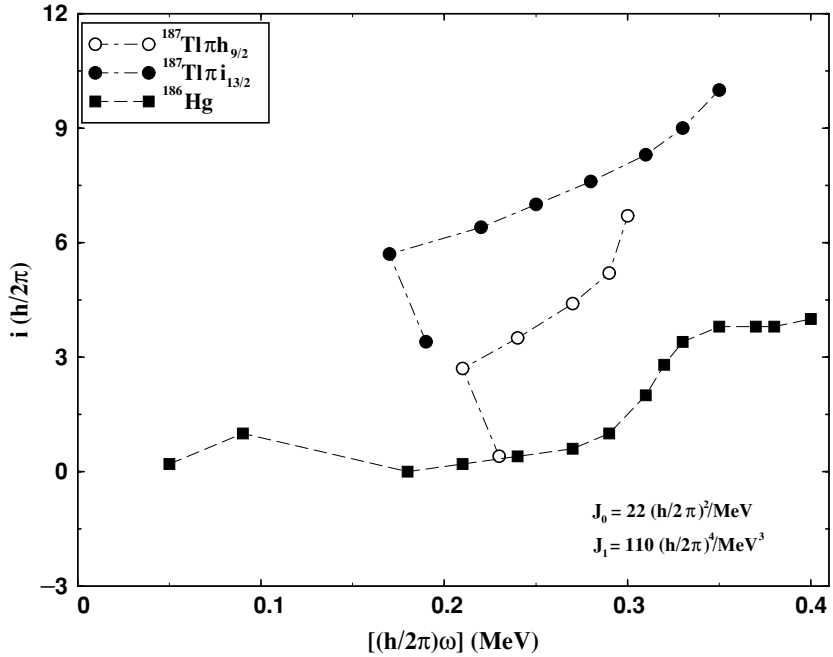

FIG. 6. The plot of aligned angular momentum (i_X) with rotational frequency ($\hbar\omega$) for prolate $\pi h_{9/2}$ and $\pi i_{13/2}$ bands in ^{187}Tl and ground state prolate band in ^{186}Hg. (Data taken from Ref. [18]).

in the two configurations. From Fig. 7(a), it is observed that in the negative parity band at a rotational frequency of $\hbar\omega = 0.16$ MeV, in addition to the stable oblate minimum, a prolate structure also builds up with $\beta_2 \sim 0.23$, $\gamma \sim 0^\circ$, which is consistent with the value of $\beta_2 \sim 0.22$ obtained experimentally by us for this band. However, for the positive parity $i_{13/2}$ band the building up of the prolate structure takes place at $\hbar\omega \sim 0.12$ MeV with $\beta_2 \sim 0.26$, $\gamma \sim 7^\circ$ as shown in Fig. 7(b), which is also in agreement with our experimental observation of $\beta_2 \sim 0.26$ for this band. The observation of a prolate structure in addition to the ground-state oblate structure for the two bands indicate that for the negative parity configuration ($h_{9/2}$) as well as for the positive parity configuration ($i_{13/2}$) the nucleus prefers an oblate shape at low frequencies, whereas

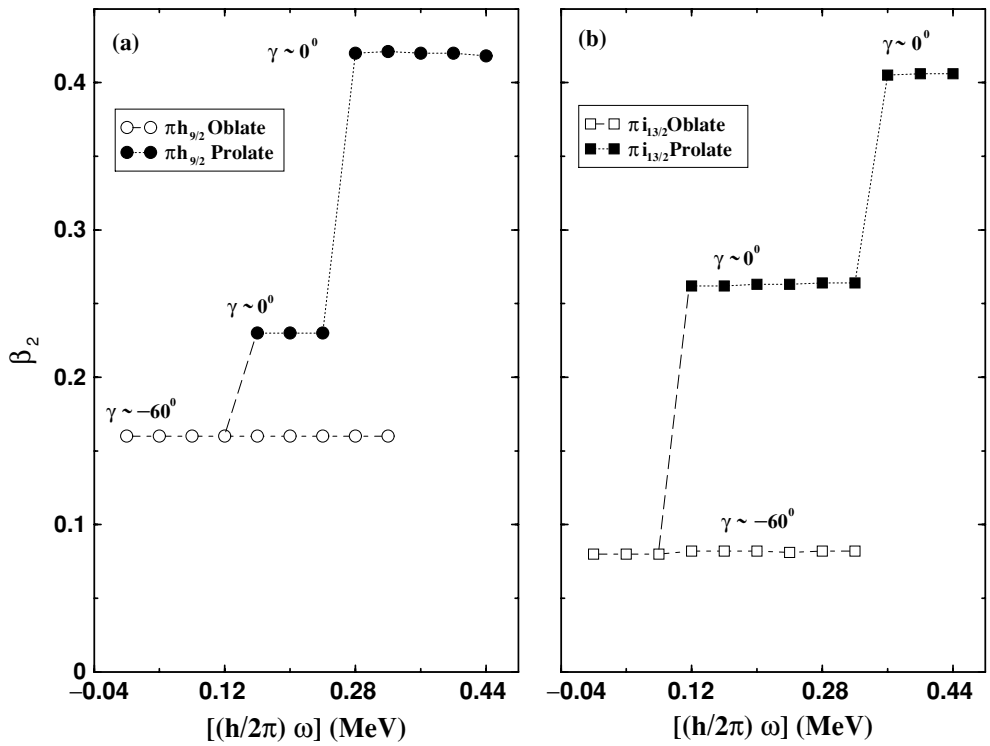

FIG. 7. Plot of the TRS calculated β_2 and γ deformation parameters as a function of the rotational frequency for the negative parity, positive signature $\pi h_{9/2}$ band and the positive parity, positive signature $\pi i_{13/2}$ band in ^{187}Tl.

at moderately higher frequencies ($\hbar\omega = 0.12$ to 0.32 MeV) it shows a mixed character with the coexistence of an oblate and a prolate shapes. At rotational frequency $\hbar\omega \sim 0.32$ MeV the nucleus assumes a highly deformed prolate shape ($\beta_2 \sim 0.41$) leading to superdeformation in both configurations.

The observed large deformations for the $h_{9/2}$ and $i_{13/2}$ prolate bands indicate that both contribute to the formation of the prolate Hg core as these bands will be lower in energy at high spins, thus ruling out the blocking hypothesis of Porquet *et al*. [14]. Also as the observed deformation of $\pi h_{9/2}[532]3/2^-$ configuration ($\beta_2 = 0.22$) is more than the predicted deformation ($\beta_2 = 0.14$) of $\pi h_{9/2}[541]1/2^-$ configuration [17], hence the prolate $h_{9/2}$ band is basically of the [532] $3/2^-$ type and not of the [541] $1/2^-$ type as predicted by Lane *et al*. [17].

V. SUMMARY

The recoil distance lifetime measurements have been carried out for the $h_{9/2}$ and the $i_{13/2}$ bands in ^{187}Tl to study the shape coexistence phenomena. The lifetimes have been found for the levels of both the negative parity positive signature $\pi h_{9/2}$ and the positive parity positive signature $\pi i_{13/2}$ bands. The transition quadrupole moment (Q_t) and the $B(E2)$ values are deduced from the measured lifetimes. For the $h_{9/2}$ band a sharp jump in the value of the average transition quadrupole moment is observed in going from the oblate configuration (2.1 eb) at a spin of $17/2^-$ to the prolate configuration (6.4 eb) at a spin of $21/2^-$. Similarly for the $i_{13/2}$ band a sudden change in the deformation is observed with the transition quadrupole moment changing from 1.8 eb at $17/2^+$ to 5.6 eb at $21/2^+$. On an average, the transition quadrupole moment of the $i_{13/2}$ band is somewhat higher than the $h_{9/2}$ band. When confirmed, this might be attributed to the higher deformation driving property of the low $K = 1/2$, $\pi i_{13/2}[660]$ configuration as compared to the $K = 3/2$, $\pi h_{9/2}[532]$ configuration. The shape coexistence picture is predicted by the TRS calculations from $\hbar\omega = 0.12$ to 0.32 MeV and is verified with the observation of a shape change in the value of transition quadrupole moment from oblate to prolate configuration for both the $i_{13/2}$ and $h_{9/2}$ bands. The calculated deformation $\beta_2 = 0.26$ at moderate frequencies for the prolate $i_{13/2}$ band and $\beta_2 = 0.22$ for the $h_{9/2}$ band is found to be in close agreement with the experimentally measured deformation that further indicate that both the configurations contribute in the formation of prolate Hg core and thus rules out the blocking hypothesis of Porquet *et al*. [14].

ACKNOWLEDGMENTS

The authors thank Professor Umesh Garg and G. Angiles for useful discussions and suggestions regarding this experiment. We are also thankful to the Pelletron crew at Nuclear Science Center, New Delhi for providing an excellent and stable beam. Thanks are also due to the UGC and CSIR—India for the financial support.

[1] D. Proetel and F. S. Stephens, Phys. Lett. **B48**, 102 (1999).
[2] R. Beraud *et al*., Nucl. Phys. **A284**, 221 (1977).
[3] J. D. Cole *et al*., Phys. Rev. C **16**, 2010 (1977).
[4] R. V. F. Janssens *et al*., Phys. Lett. **B131**, 35 (1983).
[5] W. C. Ma *et al*., Phys. Lett. **B167**, 277 (1986).
[6] M. G. Porquet *et al*., J. Phys. G **18**, L29 (1992).
[7] G. D. Dracoulis *et al*., Phys. Lett. **B208**, 365 (1988).
[8] W. C. Ma *et al*., Phys. Lett. **B139**, 276 (1984).
[9] N. Rud *et al*., Phys. Rev. Lett. **31**, 1421 (1973).
[10] J. H. Hamilton *et al*., Phys. Rev. Lett. **35**, 562 (1975).
[11] A. M. Baxter *et al*., Phys. Rev. C **48**, R2140 (1993).
[12] J. Heese *et al*., Phys. Lett. **B302**, 390 (1993).
[13] A. J. Kreiner, J. Davidson, M. Davidson, H. Moscha, L. L. Riedinger, R. C. Bingham, M. W. Guidry, and A. C. Kahler, Phys. Rev. C **38**, 2674 (1988).
[14] M. G. Porquet *et al*., Phys. Rev. C **44**, 2445 (1991).
[15] W. Reviol *et al*., Phys. Rev. C **49**, R587 (1994).
[16] G. J. Lane *et al*., Phys. Lett. **B324**, 14 (1994).
[17] G. J. Lane *et al*., Nucl. Phys. **A586**, 316 (1995).
[18] W. Reviol *et al*., Phys. Scr. Vol. **T56**, 167 (1995).
[19] T. K. Alexander and A. Bell, Nucl. Instrum. Methods **81**, 22 (1970).
[20] J. C. Wells *et al*., Report No. ORNL/TM-9105 (1985).
[21] A. Abragaam and R. V. Pound, Phys. Rev. **98**, 943 (1953).
[22] F. James and M. Roose, Comput. Phys. Commun. **10**, 343 (1975).
[23] S. K. Chamoli, P. Joshi, A. Kumar, R. P. Singh, S. Muralithar, R. K. Bhowmik, K. Z. Naik, C. R. Praharaj, and I. M. Govil, Phys. Rev. C **66**, 024307 (2002).
[24] P. Joshi, G. Mukherjee, A. Kumar, R. P. Singh, S. Muralithar, S. C. Pancholi, C. R. Praharaj, U. Garg, R. K. Bhowmik, and I. M. Govil, Phys. Rev. C **60**, 034311 (1999).
[25] P. Joshi, G. Mukherjee, A. Kumar, R. P. Singh, S. Muralithar, S. K. Chamoli, C. R. Praharaj, U. Garg, R. K. Bhowmik, and I. M. Govil, Phys. Rev. C **64**, 034303 (2001).
[26] D. Muller *et al*., Phys. Lett. **B332**, 265 (1994).
[27] P. Joshi, A. Kumar, G. Mukherjee, R. P. Singh, S. Muralithar, U. Garg, R. K. Bhowmik, and I. M. Govil, Phys. Rev. C **66**, 044306 (2002).
[28] D. Proetel *et al*., Phys. Lett. **B48**, 102 (1974).
[29] P. Ring and P. Schuck, *The Nuclear Many Body Problems* (Springer-Verlag, Berlin, 1980), p. 244.
[30] W. Nazarewicz, M. A. Riely, and J. D. Garrett, Nucl. Phys. **A512**, 61 (1990).
[31] T. R. Werner and J. Dudek, At. Data Nucl. Data Tables **59**, 1 (1995).
[32] T. R. Werner and J. Dudek, At. Data Nucl. Data Tables **50**, 179 (1992).
[33] S. G. Nilsson and I. Ragnarsson, *Shapes and Shells in Nuclear Structure* (Cambridge University Press, Cambridge, England, 1995), p. 290.
[34] V. M. Strutinsky, Yad. Fiz. **3**, 614 (1966); Nucl. Phys. **A95**, 420 (1967) .